

Article

Novel Polyamides with 5*H*-Dibenzo[*b,f*]azepin-5-yl-Substituted Triphenylamine: Synthesis and Visible-NIR Electrochromic Properties

Qingyi Lu ¹, Wanan Cai ¹, Haijun Niu ^{1,*}, Wen Wang ^{2,*}, Xuduo Bai ¹ and Yanjun Hou ¹ 

¹ Key Laboratory of Functional Inorganic Material Chemistry, Ministry of Education, Department of Macromolecular Science and Engineering, School of Chemical, Chemical Engineering and Materials, Heilongjiang University, Harbin 150086, China; qingyiluhlju@163.com (Q.L.); w.a.cai@hrbeu.edu.cn (W.C.); baixuduo@hlju.edu.cn (X.B.); houyj@hlju.edu.cn (Y.H.)

² School of Materials Science and Engineering, Harbin Institute of Technology, Harbin 150080, China

* Correspondence: niuhaijun@hlju.edu.cn (H.N.); wangwen@hit.edu.cn (W.W.); Tel.: +86-136-8450-1571 (H.N.)

Received: 29 September 2017; Accepted: 20 October 2017; Published: 23 October 2017

Abstract: In this study, a new diamine monomer, namely 4,4'-diamino-4''-(5*H*-dibenzo[*b,f*]azepin-5-yl)triphenylamine, was prepared and polymerized with four kinds of dicarboxylic acids via direct polycondensation reaction resulting in a novel series of soluble and electroactive polyamides (PAs). The tough thin films of all PAs could be solution-cast onto an indium-tin oxide (ITO)-coated glass substrate owing to the good solubility in polar organic solvents. Two pairs of obvious redox peaks for these films were observed in cyclic voltammetry (CV) with low onset potentials (E_{onset}) of 0.37–0.42 V accompanying with remarkable reversible color changes between light yellow and dark blue. A new absorption peak at around 915 nm emerged in near infrared (NIR) spectra; the increasing potential indicated that PAs could be used as a NIR electrochromic material. Moreover, the PAs showed high coloration efficiency (CE; η) in the range of 190–259 cm² C⁻¹.

Keywords: triphenylamine; 5*H*-dibenzo[*b,f*]azepine; polyamide; electrochemical

1. Introduction

Due to their significant, lasting, and reversible changes in color upon reduction or oxidation, electrochromic materials have received a great deal of attention and also play an important role in our lives via electrochromic windows, e-paper, electrochromic energy storage devices, and adaptive camouflage [1–4]. There are many chemical species frequently used for electrochromic studies, including metal coordination complexes, metal oxides, and conducting polymers (such as polyanilines) [5,6]. However, conjugated polymers always have a deep color in neutral state, which limits their use in smart window that will block the light in a dark environment. In recent years, triarylamine-based condensation-type polymers such as aromatic PAs and polyimides (PIs) have been developed to resolve the problem, and have been reported as a new and attractive family of electrochromic materials due to their mechanical flexibility, high optical contrast ratios, and long-term redox stability [7–10].

It is common knowledge that aromatic PAs have many outstanding material properties, such as high thermal stability, good electrical properties, excellent mechanical properties, and chemical resistance [11–13]. However, due to their rigid backbones and strong interchain interactions, most aromatic PAs have a high melting or softening temperature. To overcome these drawbacks, Wang et al. offer a strategy to incorporate flexible linkages, asymmetric units, or bulky pendant groups into the PAs' backbones [14–16]. In the past few years, Liou and Hsiao's groups have reported a large number

of triarylamine-based high-performance polymers [17–22]. The introduction of propeller-shaped triarylamine units into the PAs backbone as a structural modification to rigid PIs has the potential to form an amorphous structure exhibiting excellent solubility and film-forming capabilities [23–25].

On the other hand, triphenylamine (TPA) and its derivatives are widely used in hole transport materials in organic photo-electronic devices because of their stable radical cations and good hole mobility [26–28]. The introduction of TPA units into the polymers could enhance the glass transition temperature (T_g) and solution processability, and also facilitate the charge transfer (CT) behavior of polymers [29–31]. Incorporation of electron-donating substituent at the para position of TPA can afford a stable radical cation and enhance the electrochemical and electrochromic stability of the polymers, and the oxidation process is always associated with a noticeable change of color [32,33]. Recently, Feng and Zhu's groups reported that 5*H*-dibenzo[*b,f*]azepine is used as a dye-sensitized solar cells (DSSCs) [34,35]. 5*H*-dibenzo[*b,f*]azepine is a conjugated structure that will facilitate electron mobility. Inspired by these studies, 5*H*-dibenzo[*b,f*]azepine is expected to promote the electrochemical and electrochromic stability of the resulting PAs. In our study, it was demonstrated that the introduction of 5*H*-dibenzo[*b,f*]azepine as an electron donor into the backbone of PAs greatly enhanced the performance of PAs. In particular, the driving voltage of the polymers is significantly reduced, which will greatly promote the development of photoelectric materials.

In this article, a new diamine monomer and a novel series of electroactive aromatic PAs were synthesized. We make a detailed investigation of the properties of these PAs, such as organic solubility, thermal properties, and photoelectric performances.

2. Experimental

2.1. Materials

4,4'-Sulfonyldibenzoic acid (TCI), 5*H*-dibenzo[*b,f*]azepine (TCI), 2,2-bis-(4-carboxyphenyl)-hexafluoropropane (TCI), 1,4-cyclohexanedicarboxylic acid (Sinopharm Chemical Reagent Co., Ltd., Shanghai, China), 1,4-dicarboxybenzene (Sinopharm Chemical Reagent Co., Ltd., Shanghai, China), 4-fluoronitrobenzene (Sinopharm Chemical Reagent Co., Ltd. Shanghai, China), 10% palladium on charcoal (Pd/C, Acros, Geel, Belgium), and 80% hydrazine monohydrate (TCI) were used as received. *N,N*-dimethylformamide (DMF) and *N*-methyl-2-pyrrolidinone (NMP) were dried over calcium hydride overnight (for 18 h), distilled under reduced pressure (−0.1 MPa), then stored in molecular sieves in a sealed bottle before use. Tetrabutylammonium perchlorate (Bu_4NClO_4 , Acros, Geel, Belgium) was recrystallized twice from ethanol under nitrogen atmosphere and then dried before use. Other commercially available chemicals and solvents were used without further purification.

2.2. Measurements

Fourier transform infrared (FTIR) spectra were recorded on a PerkinElmer (Fremont, CA, USA) Spectrum 100 Model FT-IR spectrometer. ^1H NMR (Nuclear Magnetic Resonance), ^{13}C NMR, H-H COSY, and C-H HSQC (Heteronuclear Singular Quantum Correlation) spectra were measured by a Bruker (Rheinstetten, Germany) AVANCE 500 FT-NMR system with tetramethylsilane as an internal reference. Gel permeation chromatography (GPC) analysis was performed on a Malvern instrument (Worcestershire, UK) connected with double refractive index detector. Thermogravimetric analysis (TGA) was conducted on a PerkinElmer (Pyris 6 TGA, Fremont, CA, USA) in a nitrogen atmosphere with a heating rate of $10 \text{ K} \times \text{min}^{-1}$ and a sample weight of 8–10 mg. UV-Vis absorption spectra were recorded using a Shimadzu (Kyoto, Japan) UV-3600 spectrophotometer.

CV measurements were carried out on a CH Instruments, Inc (Shanghai, China) 660E electrochemical work station at a scan rate of 50 mV s^{-1} . A 0.1 M solution of Bu_4NClO_4 in dry acetonitrile (ACN) worked as the supporting electrolyte and a Pt wire and Ag/AgCl electrodes worked as the counter electrode and the reference electrode, respectively. The PA films that were cast on an ITO-coated glass slide were measured. The HOMO (Highest Occupied Molecular Orbital) and LUMO

(Lowest Unoccupied Molecular Orbital) levels of PAs were calculated on the premise of the absolute energy level of Fc/Fc⁺ as -4.80 eV. The density functional theory (DFT) is calculated on a computer. Geometric optimization was performed using the B3LYP functional in the Gaussian 03 program.

2.3. Synthesis of Monomers

2.3.1. 5-(4-Nitrophenyl)-5H-dibenzo[*b,f*]azepine (M1)

In a 250-mL three-neck round-bottom flask equipped with a magnetic rotor, a mixture of 2.90 g (15.0 mmol) of 5H-dibenzo[*b,f*]azepine, 0.53 g (22.0 mmol) of sodium hydride in 110 mL of dried DMF was stirred under a nitrogen atmosphere at 25 °C for 0.5 h. Then, 2.33 g (16.5 mmol) of 4-fluoronitrobenzene was added dropwise at 25 °C. The mixture was stirred in a nitrogen atmosphere at 115 °C for 24 h. After cooling to room temperature, the reaction solution was poured into 500 mL of water to precipitate the crude solid. Recrystallization from ethanol yielded the compound M1 as a yellow powder in 85.5% yield, m.p.: 169–170 °C. FTIR (KBr): 1306, 1586 ($-\text{NO}_2$ stretch) cm^{-1} . ¹H NMR (400 MHz, DMSO-*d*₆, δ , ppm): 7.98–7.96 (d, 2H, H_a), 7.67–7.65 (d, 6H, H_d + H_f + H_g), 7.56–7.52 (t, 2H, H_b), 7.03 (s, 2H, H_e), 6.26–6.28 (d, 2H, H_c).

2.3.2. 4-(5H-Dibenzo[*b,f*]azepin-5-yl)aniline (M2)

First 0.50 g of Pd/C and 3.14 g (10.0 mmol) of M1 were added into 100 mL of ethanol under nitrogen atmosphere in a round-bottom flask of 250 mL capacity. Then, 12.0 mL of hydrazine monohydrate were added dropwise, and the mixture was refluxed at 78 °C for 8 h. Then, the reaction mixture was filtered to remove Pd/C and poured into 300 mL of water; finally, compound M2 was obtained as a white solid in 62.7% yield, m.p.: 137–138 °C. FTIR (KBr): 3203, 3324 ($-\text{NH}_2$ stretch) cm^{-1} . ¹H NMR (400 MHz, DMSO-*d*₆, δ , ppm): 7.56–7.50 (m, 4H, H_d + H_f), 7.46–7.44 (t, 2H, H_g), 7.41–7.37 (t, 2H, H_e), 6.88 (s, 2H, H_c), 6.30–6.26 (d, 2H, H_b), 5.93–5.90 (d, 2H, H_a), 5.80 (s, 2H, $-\text{NH}_2$).

2.3.3. 4,4'-Dinitro-4''-(5H-dibenzo[*b,f*]azepin-5-yl)triphenylamine (M3)

A mixture of 2.84 g (10.0 mmol) of M2, 2.96 g (21.0 mmol) of 4-fluoronitrobenzene, 0.72 g (30.0 mmol) of sodium hydride, and 100 mL of dried DMF were heated under stirring at 115 °C for 24 h. Then, the reaction solution was poured into ice water to precipitate a brown product. Yield 79.2%, m.p.: 138–140 °C. FTIR (KBr): 1306, 1588 ($-\text{NO}_2$ stretch) cm^{-1} . ¹H NMR (400 MHz, DMSO-*d*₆, δ , ppm): 8.36–8.34 (d, 6H, H_a + H_h), 8.08–8.06 (d, 4H, H_f + H_i), 7.47–7.37 (d, 6H, H_b + H_g), 6.80–6.78 (d, 6H, H_e + H_c + H_d).

2.3.4. 4,4'-Diamino-4''-(5H-dibenzo[*b,f*]azepin-5-yl)triphenylamine (M4)

In a 250-mL three-neck round-bottomed flask, 1.00 g of Pd/C and 2.63 g (5.00 mmol) of M3 were added into 100 mL of ethanol under a nitrogen atmosphere. Then, 15.0 mL of hydrazine monohydrate were added dropwise, and the mixture was refluxed at 78 °C for 24 h. The solution was filtered to remove Pd/C and poured into 300 mL of water to give a white solid with a yield of 70.7%, m.p.: 160–162 °C. FTIR (KBr): 3210, 3349 ($-\text{NH}_2$ stretch) cm^{-1} . ¹H NMR (400 MHz, DMSO-*d*₆, δ , ppm): 7.55–7.50 (m, 6H, H_h + H_f), 7.47–7.45 (d, 4H, H_i), 7.40–7.36 (t, 2H, H_g), 6.88 (s, 2H, H_e), 6.32–6.29 (d, 8H, H_a + H_b), 5.97–5.94 (d, 4H, H_c + H_d), 4.39 ($-\text{NH}_2$). ¹³C NMR (100 MHz, DMSO-*d*₆, δ , ppm): 144.43 (C¹), 140.94 (C⁵ + C⁸), 140.42 (C⁹), 136.89 (C⁴), 131.09 (C³ + C⁶ + C⁷), 130.89 (C¹⁵), 130.86 (C¹⁴), 130.24 (C¹³), 127.27 (C¹²), 115.03 (C¹⁰), 113.45 (C²).

2.4. Synthesis of PAs

The synthesis of PA-a was used as an example to illustrate the general synthetic procedure. In a typical procedure, a mixture of 0.12 g (1.1 mmol) of the 1,4-cyclohexanedicarboxylic acid, 0.51 g (1.1 mmol) of M4, 0.13 g of calcium chloride (CaCl₂), 1.00 mL of triphenyl phosphite, 0.50 mL of pyridine, and 1.50 mL of NMP was heated with stirring at 120 °C for 3 h. After cooling to room

temperature, the solution was poured slowly into 250 mL of methanol, which produced a stringy, fiber-like precipitate. The resulting polymer was washed thoroughly with hot water and methanol, and then with NMP/methanol for further purification (70.8% yield). FTIR (KBr): 3315 (amide N–H stretch), 1667 (amide C=O stretch) cm^{-1} . ^1H NMR (400 MHz, $\text{DMSO-}d_6$, δ , ppm): 9.70 (amide N–H), 8.21–6.65 (aromatic ring of benzene).

Synthesis of PA–b. Yield: 69.6%. FTIR (KBr): 3301 (amide N–H stretch), 1664 (amide C=O stretch) cm^{-1} . ^1H NMR (400 MHz, $\text{DMSO-}d_6$, δ , ppm): 10.26 (amide N–H), 8.18–6.42 (aromatic ring of benzene).

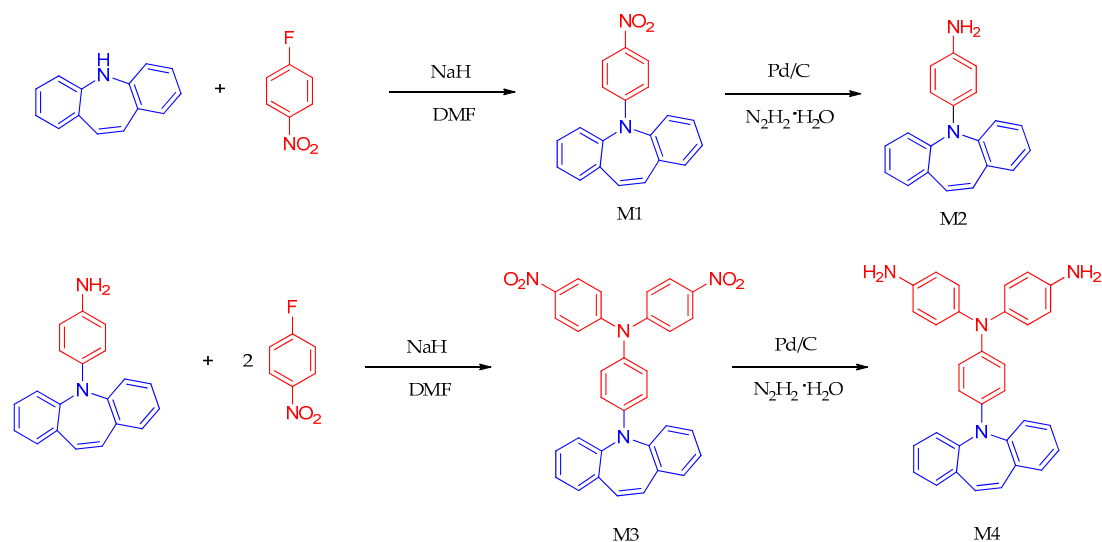
Synthesis of PA–c. Yield: 71.3%. FTIR (KBr): 3313 (amide N–H stretch), 1668 (amide C=O stretch) cm^{-1} . ^1H NMR (400 MHz, $\text{DMSO-}d_6$, δ , ppm): 10.29 (amide N–H), 8.19–6.41 (aromatic ring of benzene).

Synthesis of PA–d. Yield: 78.2%. FTIR (KBr): 3315 (amide N–H stretch), 1665 (amide C=O stretch) cm^{-1} . ^1H NMR (400 MHz, $\text{DMSO-}d_6$, δ , ppm): 10.34 (amide N–H), 8.18–6.71 (aromatic ring of benzene).

3. Results and Discussion

3.1. Monomer and Polyamide Synthesis

The synthetic routes for the monomers are shown in Scheme 1. The new diamine M4 was synthesized via a four-step route. M4 was prepared through the sodium hydride-mediated nucleophilic displacement reaction of M3 with 4-fluoronitrobenzene, followed by a hydrazine Pd/C-catalyzed reduction. FTIR (Figure A8) and ^1H NMR (Figures A1–A3) spectroscopic techniques were used to identify the structures of the intermediate compounds M1, M2 and M3. The spectra of IR and ^1H NMR agree well with the carbon and proton of the proposed molecular structure. To our knowledge, M4 was first reported in this paper, and it was characterized thoroughly. As shown in Figure A8, the characteristic bands of nitro groups at around 1306 and 1588 cm^{-1} disappeared after the reduction reaction. Meanwhile, typical N–H stretching absorptions pairs corresponding to the amino group appeared in the region of 3210 and 3349 cm^{-1} . Furthermore, as shown in Figure 1, the ^1H NMR, ^{13}C NMR, H–H COSY, and C–H HSQC spectra of the diamine monomer M4 further confirm that the target diamine monomer has been synthesized successfully.



Scheme 1. Synthetic route to the diamine monomer M4.

According to the phosphorylation technique first described by Yamazaki and co-workers (as shown in Scheme 2), we synthesized a series of novel PAs by using the same diamine monomer M4 with dicarboxylic acids a–d with triphenyl phosphite and pyridine as the condensing agents. After the raw materials were put into the reactor, the solution became viscous. We poured the solution into methanol, then the PAs precipitated in a fiber-like form. IR and NMR spectroscopy have confirmed

that PAs have been successfully synthesized. The synthesis of PA-a, used as an example, exhibited the characteristic IR absorption bands of the amide group at 1667 (amide C=O) and 3315 (amide N-H) cm^{-1} (Figure A9). The PAs were also confirmed by ^1H NMR spectra, with amide resonance peaks appearing around 9.0–11.0 ppm (Figures A4–A7).

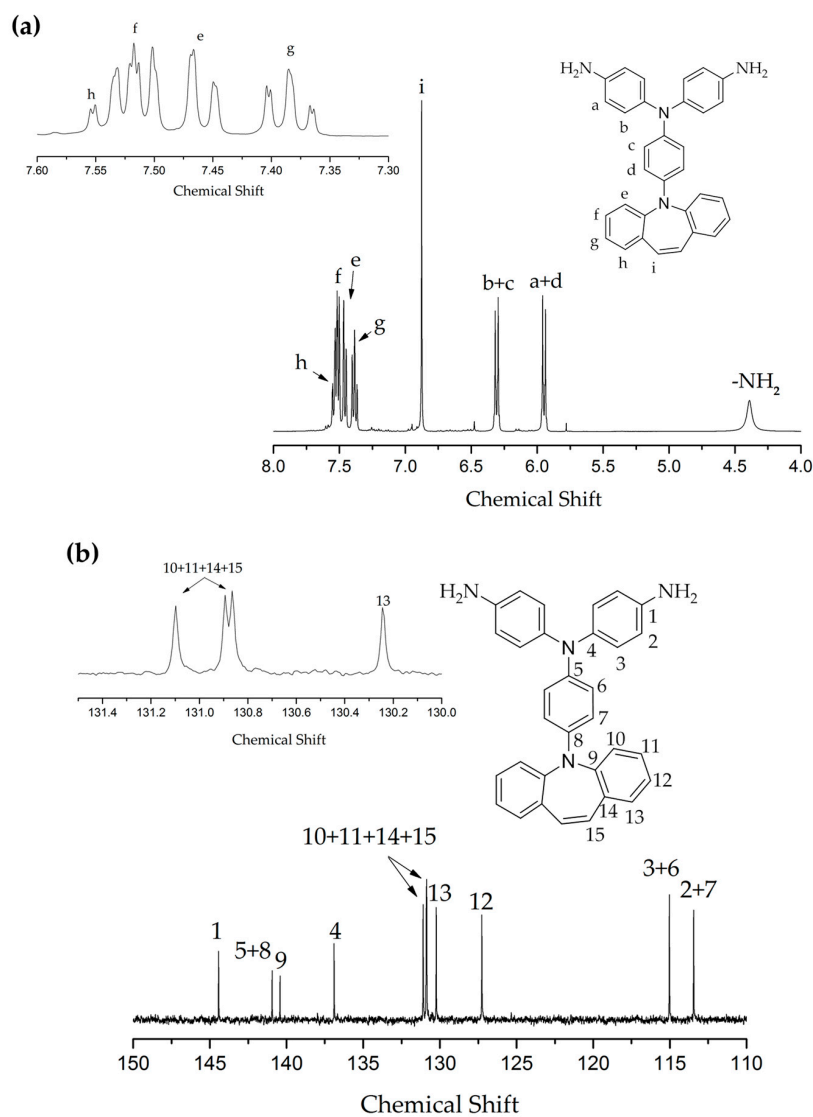
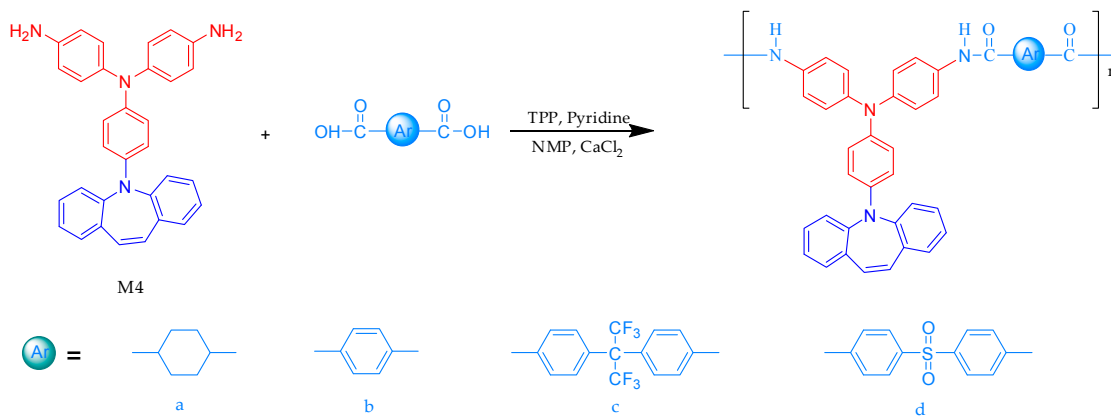


Figure 1. Cont.

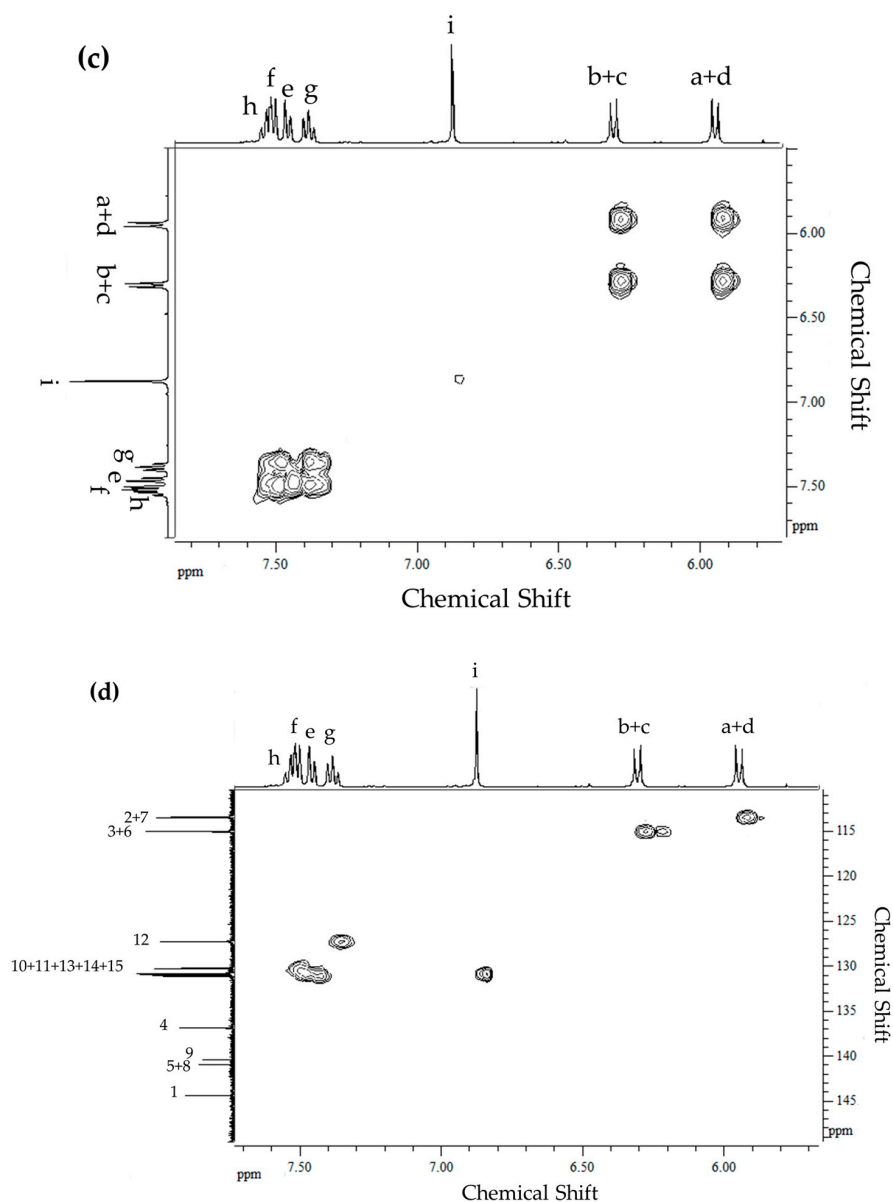


Figure 1. (a) ^1H -NMR; (b) ^{13}C -NMR; (c) H-H COSY; and (d) C-H HSQC spectrum of M4 in $\text{DMSO-}d_6$.

3.2. Solubility and Thermal Properties

The solubility tests of these PAs in several organic solvents were investigated by dissolving 20 mg sample in 2 mL of organic solvents. These PAs exhibited excellent solubility in polar organic solvents. All the PAs could be dissolved in polar solvents such as NMP, *N,N*-dimethylacetamide (DMAc), DMF, and dimethyl sulfoxide (DMSO) at room temperature, which is favorable for fabricating large-area thin film devices through convenient spin-coating processes for practical applications.

The thermal properties of these PAs were investigated by TGA measurements. In addition, the thermal performance data of the polymer are shown in Table 1. During the decomposition processes in the TGA curves (Figure A10), the 10% weight losses temperatures in nitrogen atmospheres were recorded in the range of 294–326 °C. The char yield was 55–64%. Such high char yield is due to the numerous aromatic rings in the polymeric construction. For four different PAs, the order of T_d and char yield is presented: PA-a = PA-b = PA-d > PA-c and PA-a > PA-d > PA-b > PA-c. So the stability of the polymer PA-c is worse than the other three. The reason for this phenomenon may be that the rigidity of PA backbone is weakened due to the existence of $-\text{CF}_3$. Although the C-F bond

of the PA-c is strong, the $-\text{CF}_3$ group falls off when heated. M_w , M_n and polydispersity (PDI) of PAs were determined by GPC technology.

Table 1. Thermal properties and molecular weights of the PAs.

Polymer Code	T_d ($^{\circ}\text{C}$) 10%	Char Yield (%)	M_w (Da)	M_n (Da)	PDI
PA-a	326	64	1.40×10^4	1.11×10^4	1.26
PA-b	326	58	1.33×10^4	1.05×10^4	1.27
PA-c	294	55	1.58×10^4	1.34×10^4	1.18
PA-d	326	59	1.34×10^4	1.12×10^4	1.20

3.3. Optical Properties and Electrochromic Properties

In this part, the optical properties of PAs are investigated by UV-Vis and photoluminescence (PL) techniques and the PA-a and PA-b are taken as two representative PAs. As shown in Table 2, the maximum absorption bands of the PAs in solution (DMSO, 1×10^{-5} M) and the PAs in films were located at 291–299 nm and 304–352 nm, respectively, which is caused by the $\pi-\pi^*$ transition of the TPA structure [36–38]. In Figure 2, the PA-a solution emitted a stronger fluorescence than the PA-b solution at 365 nm UV lamp irradiation and the semi-aromatic polymer PA-a ($\Phi_{\text{PL}} = 14.94\%$) exhibited a higher fluorescence quantum yield as compared to the aromatic polymer PA-b ($\Phi_{\text{PL}} = 0.93\%$). The cause for this phenomenon is that the aliphatic structure on the PA-a backbone effectively reduces the charge transfer.

Table 2. Optical properties of PAs.

Polymer Code	In Solution λ (nm)			As Film λ (nm)	
	Abs Max	PL Max	ϕ_{PL} (%)	Abs Max	Abs Onset
PA-a	299	415	14.94	332	394
PA-b	293	354	0.93	304	468
PA-c	291	352	1.12	352	436
PA-d	293	352	0.96	333	430

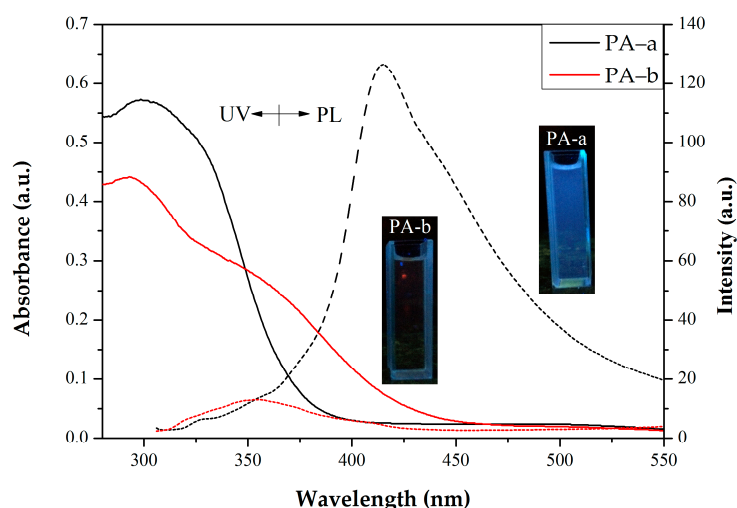


Figure 2. UV-vis (the solid line) and PL (the dotted line) spectra of the PA-a and PA-b in DMSO solutions (1×10^{-5} M) with inset taken under irradiation of 365 nm UV light.

The results of CV testing are summarized in Table 3. As shown in Figure 3, two pairs of reversible redox waves were observed in these polymers. PA-a is used as an example to illustrate electrochemical

performance. When the voltage reached 0.62 V, the first oxidation peak observed can be ascribed to oxidation of the electron-rich nitrogen atom in the TPA core and the film changing from light yellow to green. When the voltage reached 1.13 V, a second oxidation peak was observed. Upon oxidation, the polymer film changed color from green to dark blue. Furthermore, these polymers have onset potentials of the oxidation process range from 0.37 to 0.42 V. The E_{onset} value is lower for PAs than other double TPA structures [38].

Table 3. Electrochemical properties of PAs.

Polymer Code	Oxidation Potential (V)			E_g^{opt} (eV) ^c	Energy Levels (eV)	
	E_{onset}	$E_{1/2}^{\text{ox1}}$	$E_{1/2}^{\text{ox2}}$		HOMO ^a	LUMO ^b
PA-a	0.37	0.52	0.98	3.15	−4.87	−1.72
PA-b	0.39	0.54	1.02	2.65	−4.89	−2.24
PA-c	0.42	0.56	1.02	2.84	−4.91	−2.07
PA-d	0.42	0.56	1.02	2.88	−4.91	−2.03

^a $E_{\text{HOMO}} = -(E_{1/2} \text{ vs. Ag/AgCl} + 4.80 - E_{1/2, \text{ferrocene}})$ eV. Ferrocene was used as an external reference for calibration ($E_{1/2, \text{ferrocene}} = +0.45$ V vs. Ag/AgCl) in $\text{Bu}_4\text{NClO}_4/\text{ACN}$; ^b $E_{\text{LUMO}} = E_{\text{HOMO}} + E_g^{\text{opt}}$; ^c $E_g^{\text{opt}} = 1240/\lambda_{\text{onset}}$.

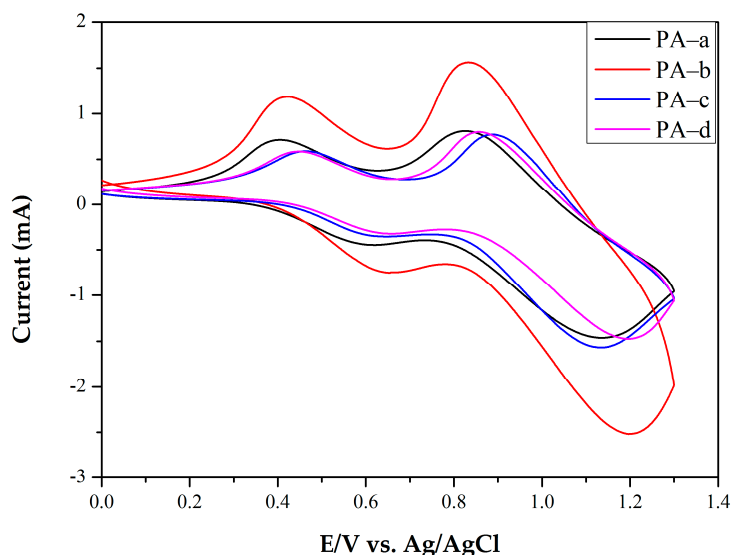


Figure 3. CV diagrams of PAs coated on ITO-coated glass slides in 0.1 M $\text{Bu}_4\text{NClO}_4/\text{ACN}$ solution at a scan rate of 50 mV s^{-1} .

3.4. Quantum Chemistry Calculation

The HOMO and LUMO values for these PAs were calculated to be in the range of -4.87 to -4.91 eV and -1.72 to -2.24 eV, respectively. However, as shown in Figure 4, the theoretical calculation was calculated to be the range of $-4.72 \sim -4.88$ eV and $-0.60 \sim -2.59$ eV. This bias may be due to the fact that the theoretical data is calculated for the monomer, not the long chain polymer. In addition, the experimental data were obtained from polymers, which are influenced by the interaction of solvent and electrolyte.

3.5. Spectroelectrochemical and Electrochromic Properties

The electrochromism properties of PA films were investigated by UV-Vis–NIR (Near Infrared) spectroscopy, and their absorption profiles were monitored with a UV-Vis spectrometer at different applied potentials. The electrode preparations and solution conditions were identical to those used in CV. The films of all PAs exhibited strong absorption at wavelengths around 304 to 412 nm in the neutral form. Upon oxidation, the main band located at around 390 to 918 nm grew.

As a typical example, the spectral changes of PA-b at various applied potentials are shown in Figure 5. In the neutral form, the film exhibited strong absorption at wavelengths around 304 nm due to the $\pi-\pi^*$ transition of the TPA group. When the applied potentials increased from 0 to 0.6 V, the absorption peak of PA at 304 nm decreased gradually, whereas two new bands grew at 390 and 914 nm, and the absorption at 914 nm was caused by the charge transfer effect (IVCT). As the applied voltage was raised to 1.2 V, the resulting spectrum did not change significantly due to TPA having been completely oxidized.

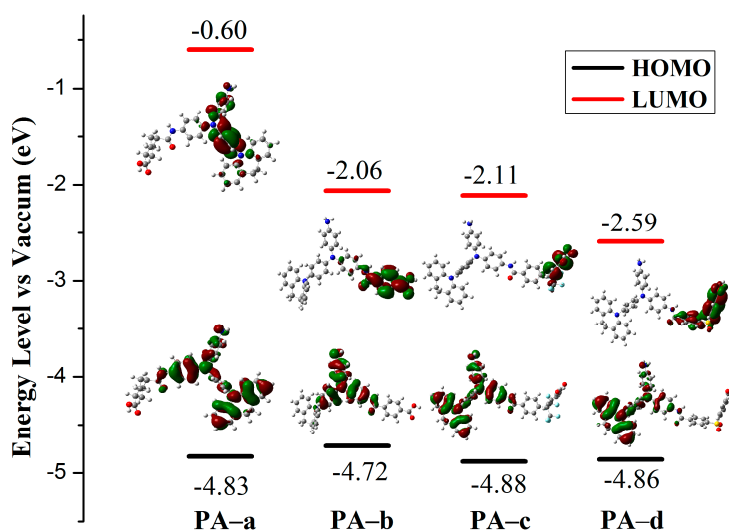


Figure 4. The frontier molecular orbitals computed for PAs at the B3LYP/6-31G.

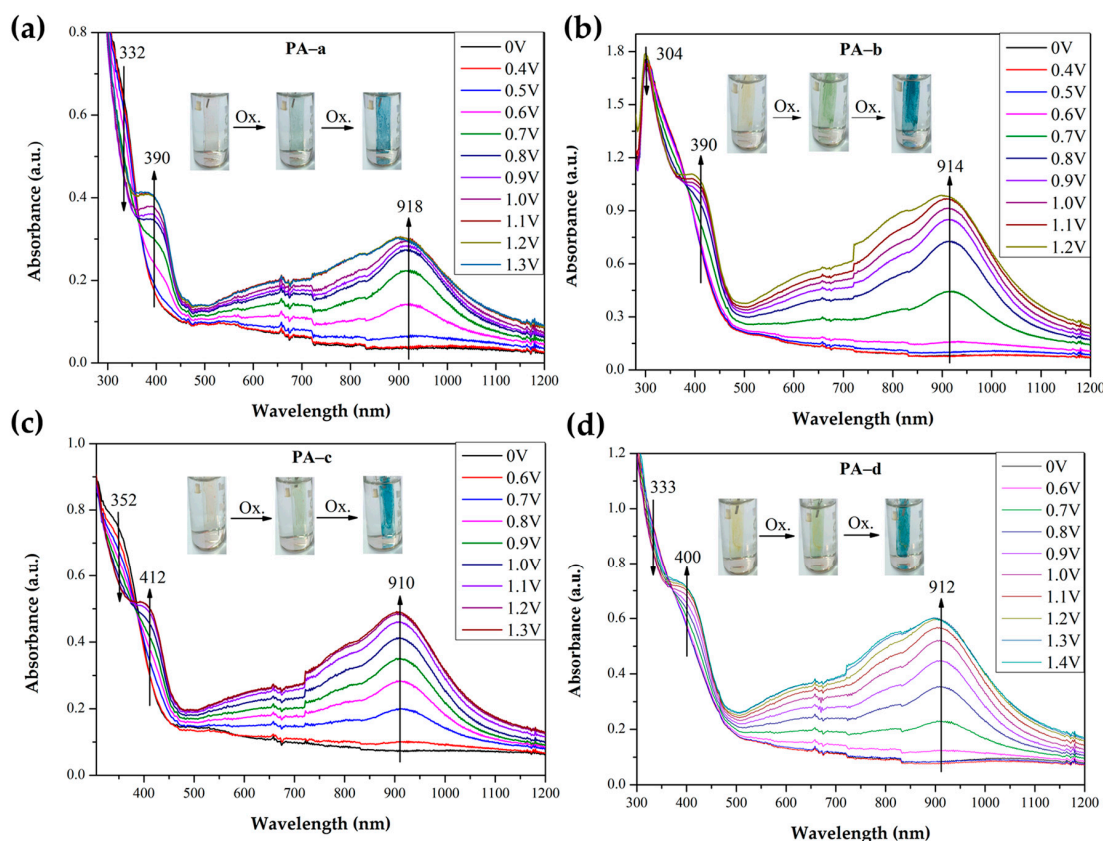


Figure 5. The electronic absorption spectrum of film of PA-a (a); PA-b (b); PA-c (c) and PA-d (d) was carried out in 0.1 M $\text{Bu}_4\text{NClO}_4/\text{ACN}$ as the supporting electrolyte.

The stability, response time, and color efficiency are important parameters for an electroactive polymer film, thus it is necessary for the electrochromic switching to be studied further. We carried out electrochromic switching studies for the PA films to record the percent transmittance changes ($\Delta T\%$) of dependence on time at their absorption maximum. The response time is determined by changing the step potential between the neutral and oxidized states, which is required to reach 90% of all the changes in absorbance after switching potential. The relevant time is displayed in Table 4. Figure 6 depict the optical transmittance of polymer films at 918 nm, 914 nm, and 910 nm as a function of time by applying square-wave potential steps between 0 and 1.1 V for a pulse time of 10 s. The electrochromic coloration efficiency (CE: η) is one of the important characteristics of electrochromic materials. CE can be calculated using the related equations. After continuous cyclic scans between 0.0 V and 1.1 V in 600 s, all polymer films still exhibited excellent stability and good stability of electrochromic characteristics, indicating that the film was very stable.

Table 4. Electrochromic properties of PAs.

Polymer Code	λ_{\max} (nm)	ΔT (%)	Response Time		ΔOD	Q_d (mC cm ⁻²)	CE (cm ² C ⁻¹)
			t_c (s)	t_b (s)			
PA-a	918	61	5.4	4.2	0.580	3.059	190
PA-b	914	74	5.7	4.7	0.820	3.987	206
PA-c	910	58	4.9	5.8	0.599	2.636	227
PA-d	912	70	6.1	5.5	0.822	3.172	259

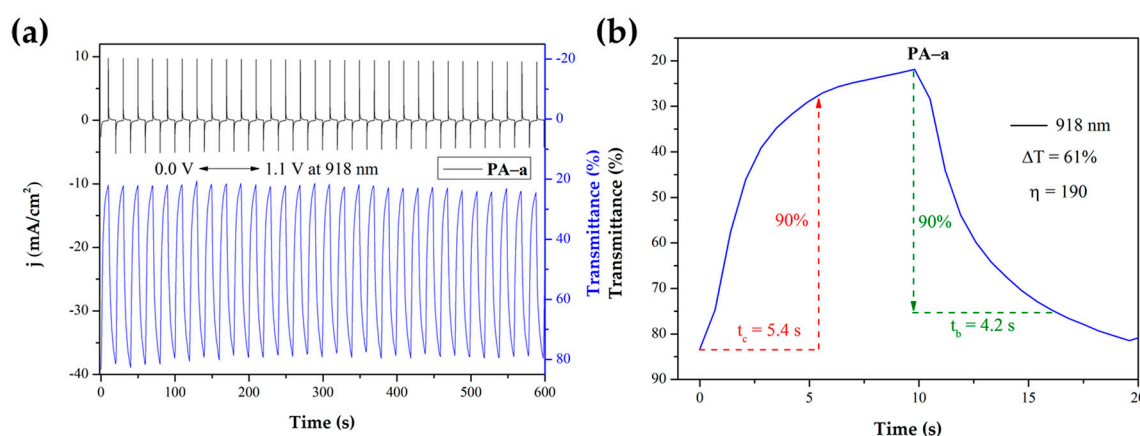


Figure 6. Dynamic changes of the transmittance and current (a) and optical switching (b) of PA-a.

Take a typical example, the PA-a revealed a satisfactory switching time of 5.4/4.2 s for the coloring/bleaching process. The optical contrast, measured as $\Delta T\%$ between neutral and oxidized state, was found to be 61% for PA-a. The CE of PA-a film was calculated to be 190 cm² /C (at 918 nm).

3.6. Photoelectrical Properties

To enlarge the application range of PAs, we further studied the photovoltage characteristics of the PAs. Switching the light on and off many times determined the reversible rise/decay process of the photovoltage response. We placed the films in a 0.2 M Bu₄NClO₄/ACN electrolyte solution and illuminated them with a 500 W xenon arc lamp (white light intensity of 150 mW cm⁻²). As shown in Figure 7, the photoelectric response was stable despite the light switching on and off many times. When the light is turned on, the photoelectric voltage immediately increases to the maximum. On the contrary, after the light is turned off, the photoelectric voltage drops sharply to the original state. It can be observed that other PAs have a similar trend (see Figure A11). The observation result can be explained by the fact that the photo-generated electrons are transported from the lowest unoccupied molecular orbital to the conduction band of the ITO surface, and then moved to the external circuit,

where the electron migration causes the change in photovoltage [39]. Therefore, these PAs can be potential materials in the photoelectric conversion of material or photodetector fields.

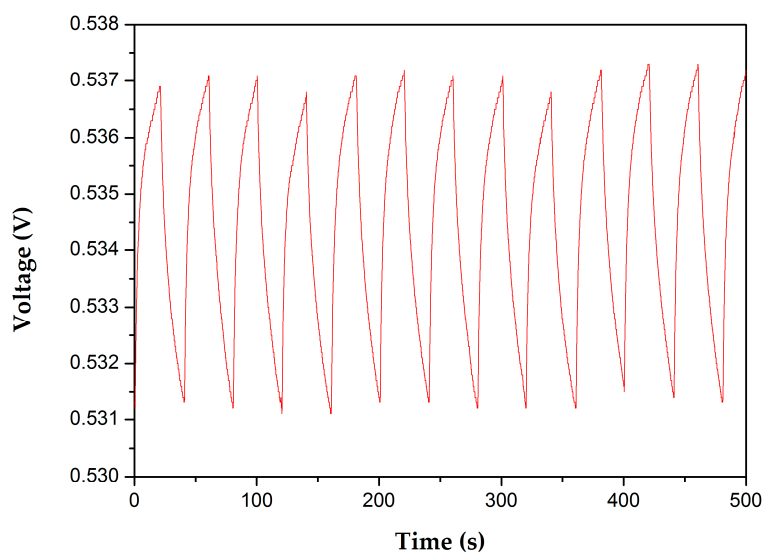


Figure 7. A typical photovoltaic response for PA-c film immobilized on ITO glass upon exposure to light with switching at room temperature.

3.7. Electrofluorochromic Performance

Electrofluorescent measurements were carried out to evaluate the optical properties in the way that Sun has reported [25]. As shown in Figure 8, the fluorescence changes under a series of positive potentials recorded to demonstrate its electrofluorochromic switching properties. The dynamic response behavior was examined by oxidation steps between 0.0 and 1.2 V. When we gradually increased the voltage, the fluorescence value of the polymer changed. A similar trend was observed for the other PAs (Figure A12). This can be attributed to the changes of the effective fluorescence quencher (TPA^+) in the polymer.

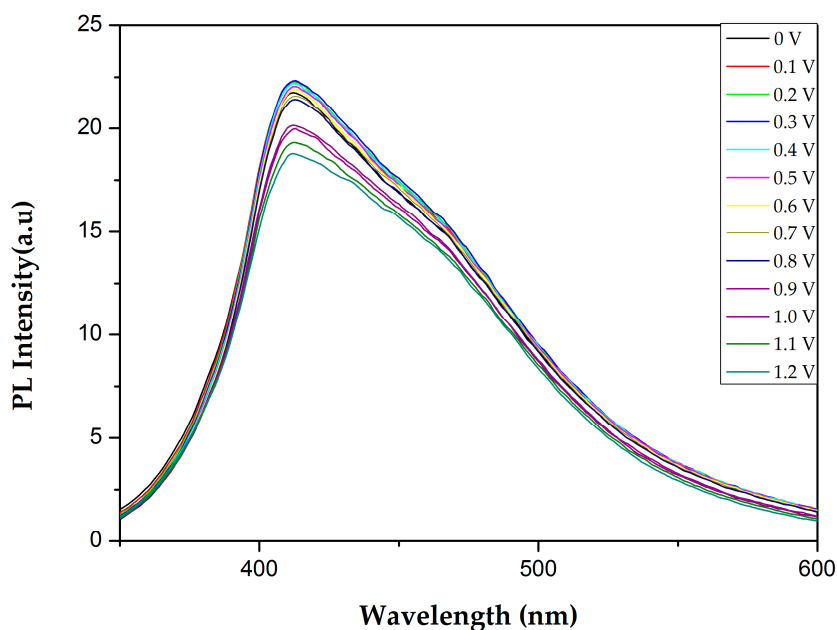


Figure 8. Fluorescence spectra changes of PA-a film upon different applied potentials from 0.0 to 1.2 V.

4. Conclusions

In summary, a series of novel electroactive PAs with 5*H*-dibenzo[*b,f*]azepin-5-yl-substituted triphenylamine have been successfully synthesized. They all exhibited good solubility in common organic solvents as well as excellent electrochemical properties, and could afford flexible and strong films with good mechanical properties. The introduction of a 5*H*-dibenzo[*b,f*]azepin-5-yl group substituent on the TPA unit greatly lowered the oxidation potentials of the PAs and enhanced the electrochemical and electrochromic stability of the PAs. From the CV curve can be seen two obvious pairs of redox peaks, and the process of oxidation from yellow to green and then into a dark blue. These polymers also revealed high optical contrast, high coloration efficiency, and good cycling stability. Thus, these new PAs can be good candidates for use in optoelectronics applications.

Acknowledgments: The authors are grateful for the support of the National Natural Science Foundation of China (grant Nos. 51773053, 51527804, 51373049, 51372055, and 21372067); Reserve Talented Person of Harbin (2015RAXXJ015) and the Natural Science Foundation of Heilongjiang Province of China (B2017010).

Author Contributions: Haijun Niu and Wen Wang conceived and designed the experiments; Qingyi Lu and Wanan Cai performed the experiments; Xuduo Bai and Yanjun Hou analyzed the data; Qingyi Lu wrote the paper.

Conflicts of Interest: The authors declare no conflict of interest. The founding sponsors had no role in the design of the study; in the collection, analyses, or interpretation of data; in the writing of the manuscript, and in the decision to publish the results.

Appendix A

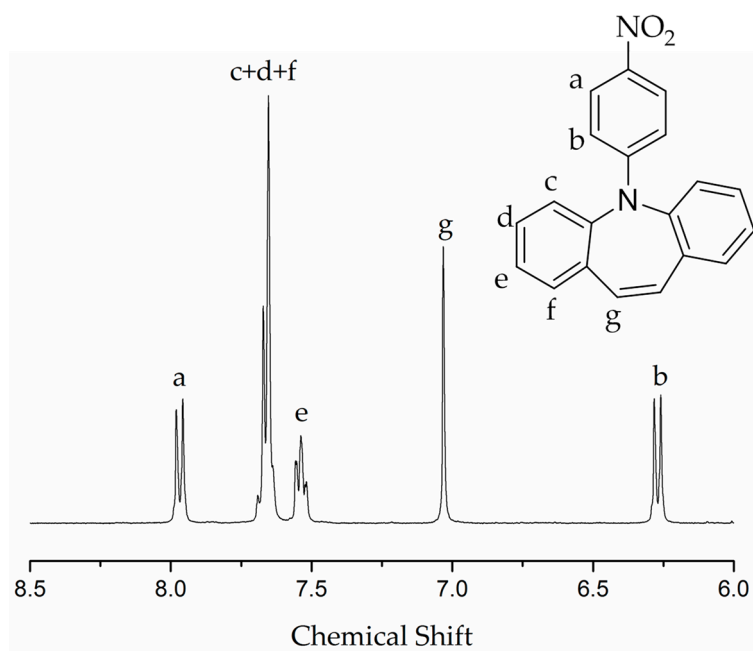


Figure A1. ¹H NMR spectrum of M1 in DMSO-*d*₆.

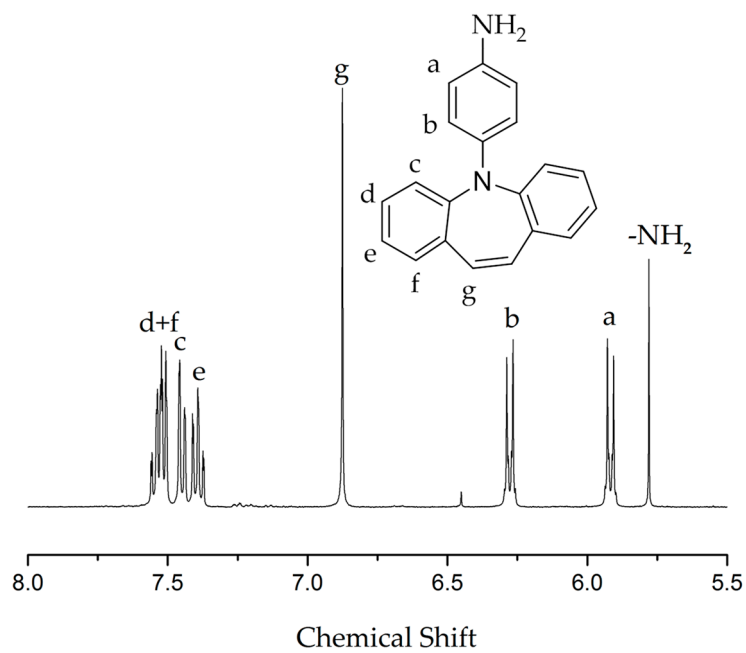


Figure A2. ¹H NMR spectrum of M2 in DMSO-*d*₆.

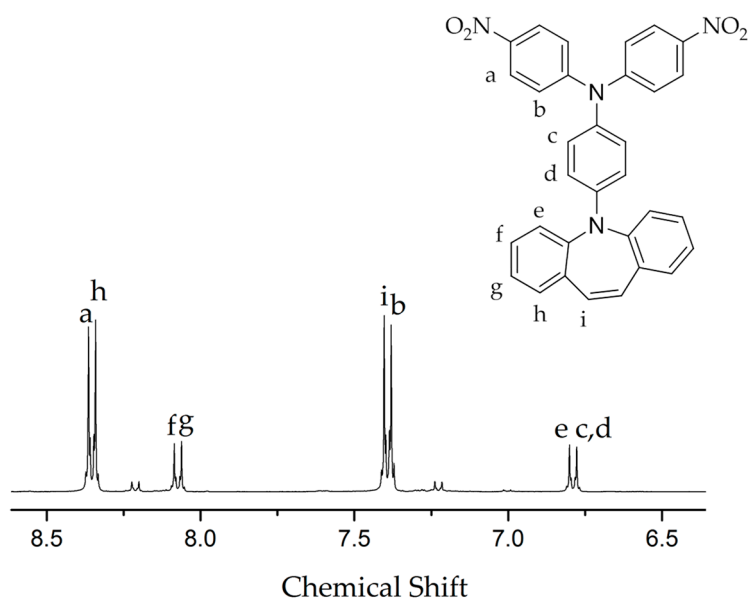


Figure A3. ¹H NMR spectrum of M3 in DMSO-*d*₆.

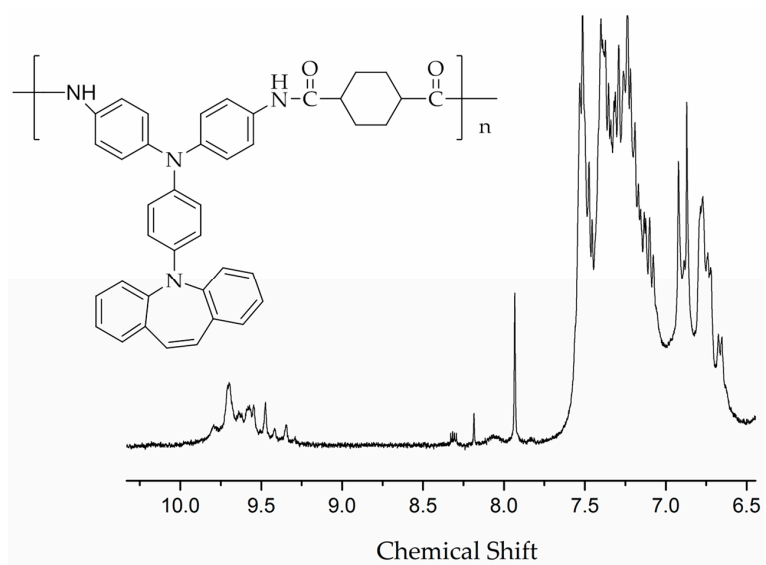


Figure A4. ^1H NMR spectrum of PA-a in $\text{DMSO-}d_6$.

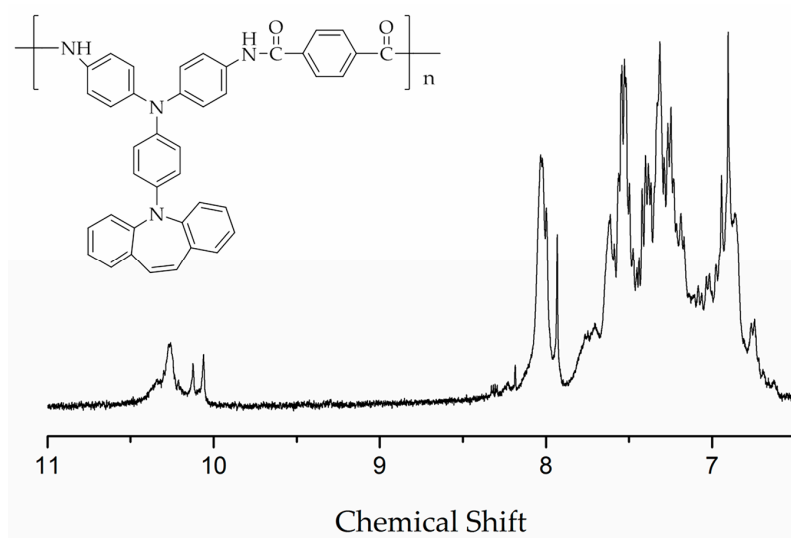


Figure A5. ^1H NMR spectrum of PA-b in $\text{DMSO-}d_6$.

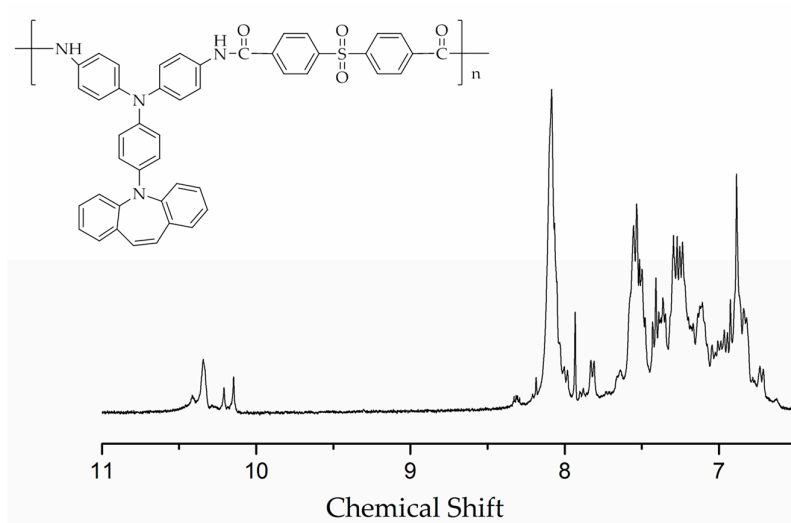


Figure A6. ^1H NMR spectrum of PA-c in $\text{DMSO-}d_6$.

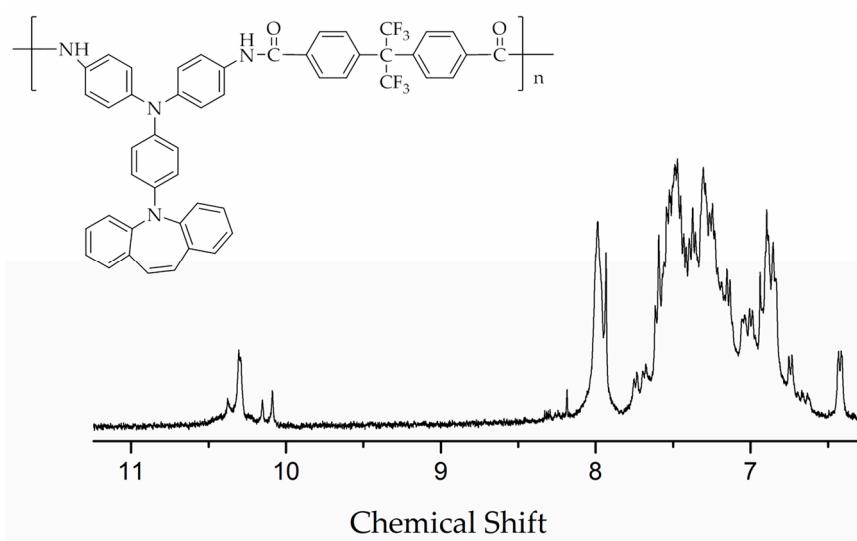


Figure A7. ¹H NMR spectrum of PA-d in DMSO-*d*₆.

Appendix B

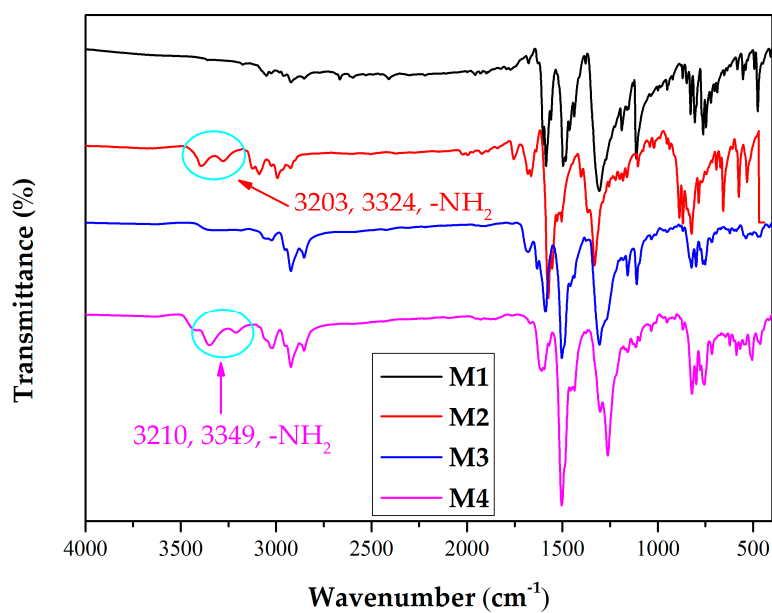


Figure A8. IR of monomers.

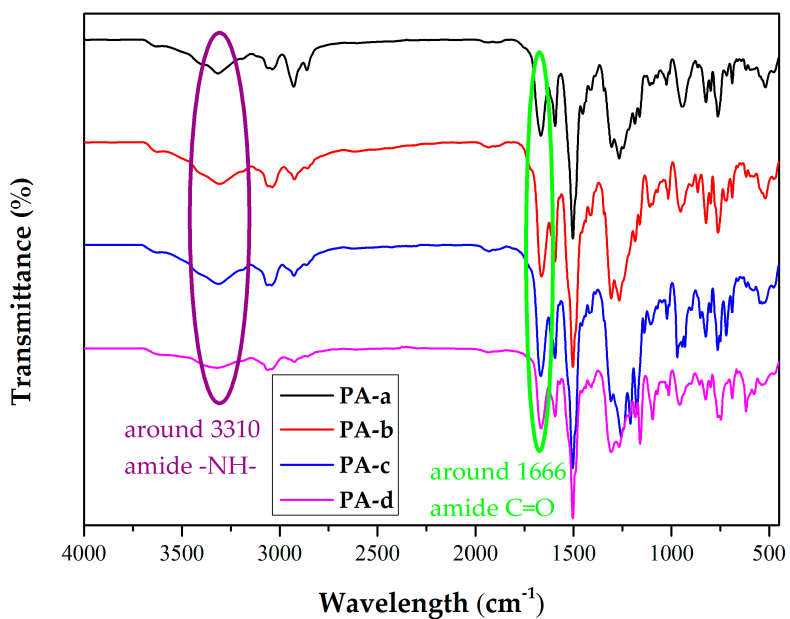


Figure A9. IR of PAs.

Appendix C

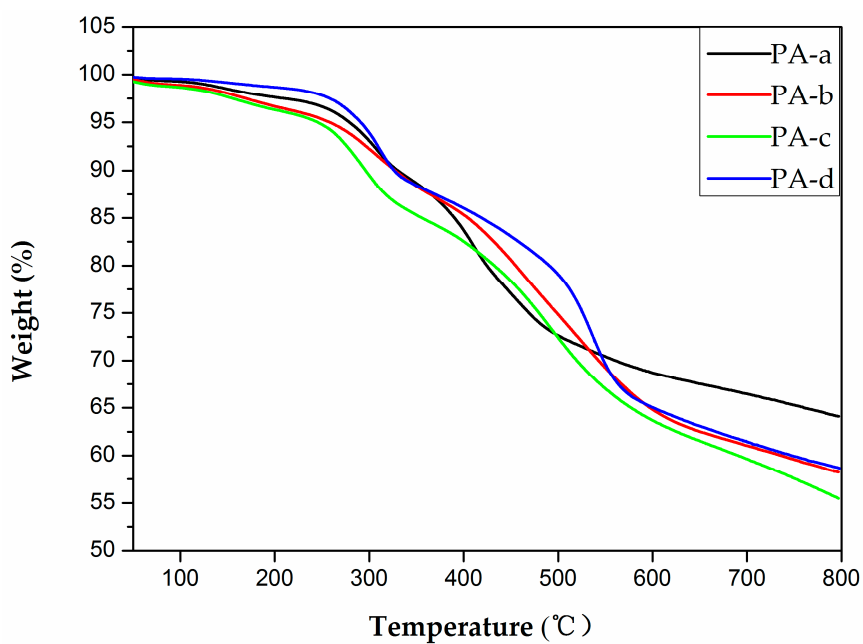


Figure A10. TGA of PAs.

Appendix D

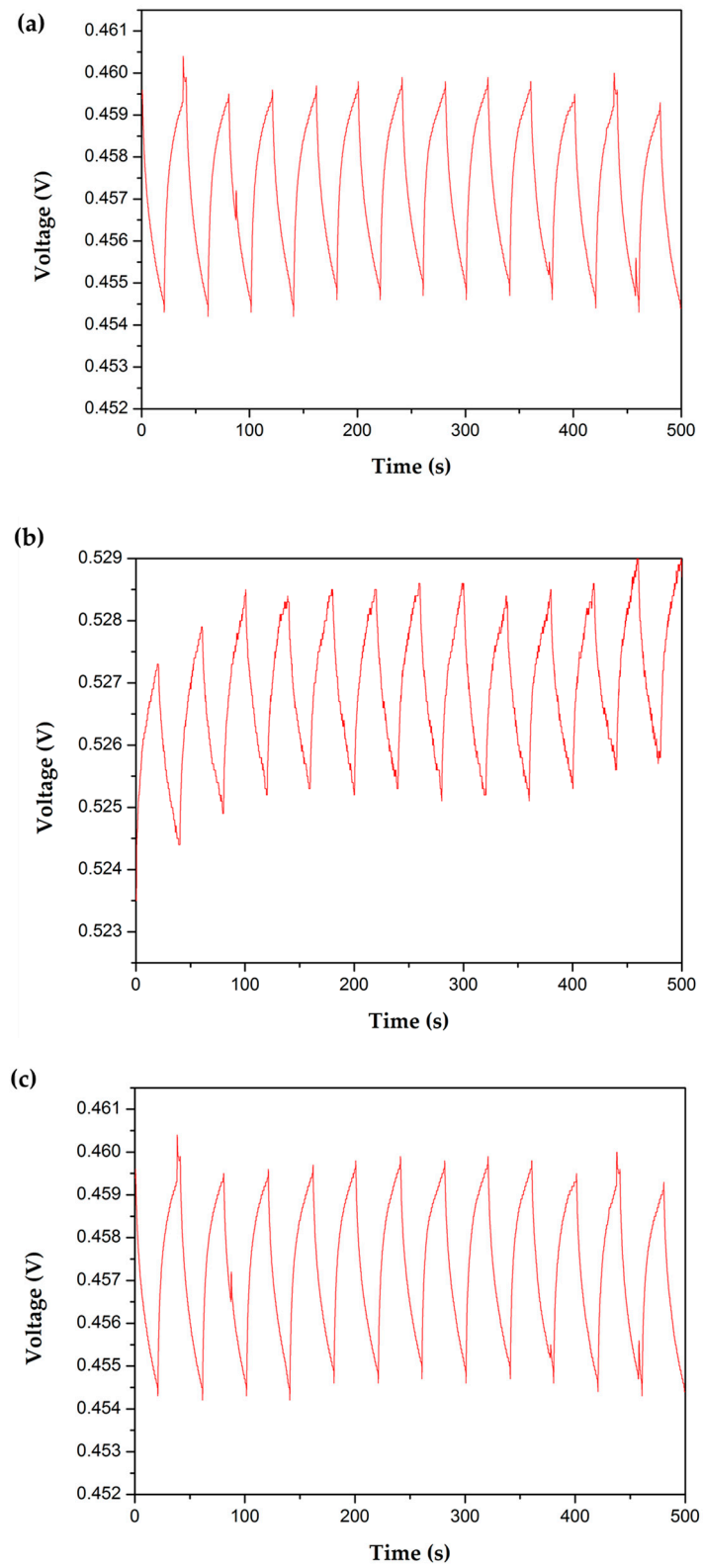


Figure A11. A typical photovoltaic response for PA-a (a); PA-b (b); and PA-d (c) film immobilized on ITO glass upon exposure to light with switching at room temperature.

Appendix E

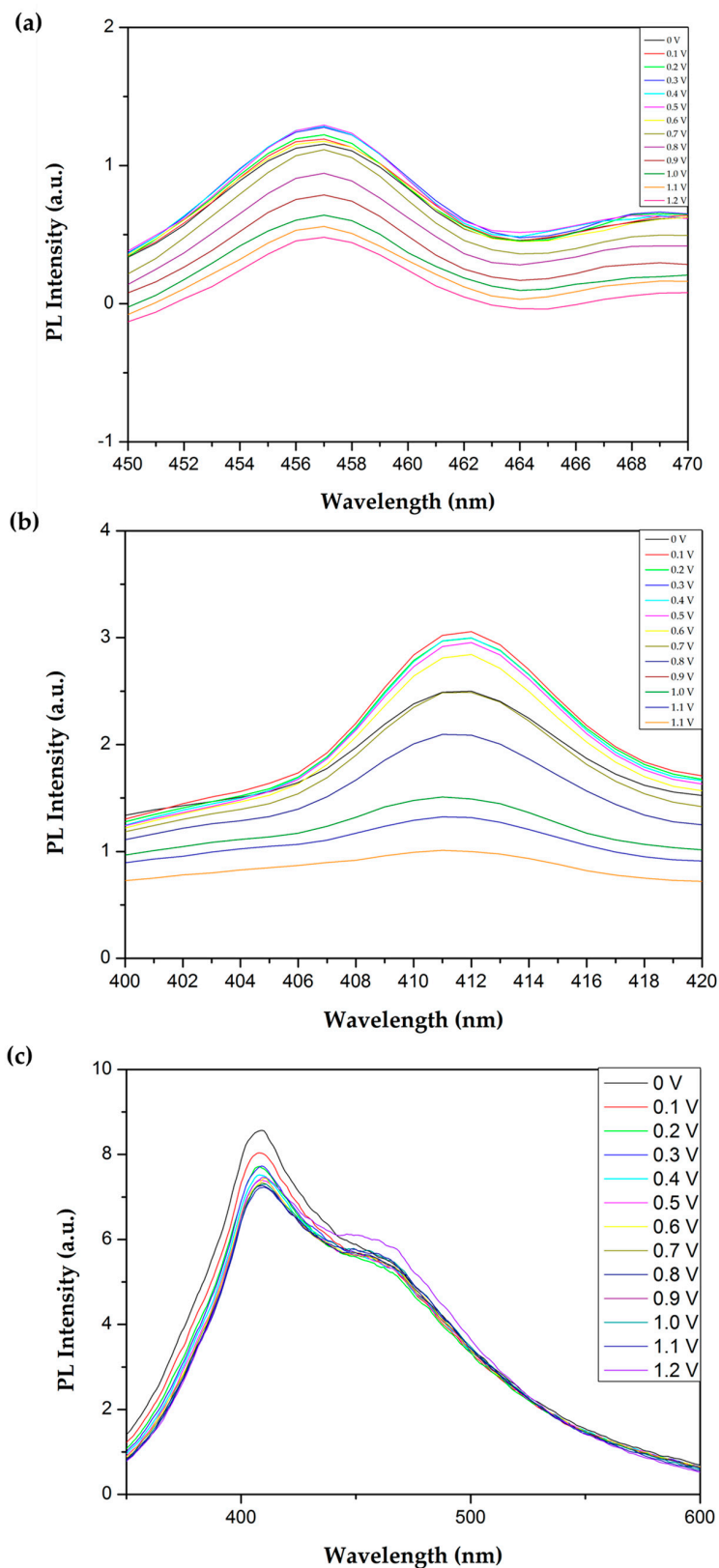


Figure A12. Fluorescence spectra changes of PA-b (a); PA-c (b); and PA-d (c) film upon different applied potentials from 0.0 to 1.2 V.

References

1. Hsiao, S.H.; Chang, P.C.; Wang, H.M.; Kung, Y.R.; Lee, T.M. Synthesis of a new class of triphenylamine-containing poly(ether-imide)s for electrochromic applications. *J. Polym. Sci. Part A Polym. Chem.* **2014**, *52*, 825–838. [[CrossRef](#)]
2. Yen, H.J.; Tsai, C.L.; Chen, S.H.; Liou, G.S. Electrochromism and nonvolatile memory device derived from triphenylamine-based polyimides with pendant viologen units. *Macromol. Rapid Commun.* **2017**, *38*, 1600715. [[CrossRef](#)] [[PubMed](#)]
3. Beaujuge, P.M.; Reynolds, J.R. Color control in π -conjugated organic polymers for use in electrochromic devices. *Chem. Rev.* **2010**, *110*, 268–320. [[CrossRef](#)] [[PubMed](#)]
4. Hsiao, S.H.; Chen, Y.Z. Electrochemical synthesis of stable ambipolar electrochromic polyimide film from a bis(triphenylamine) perylene diimide. *J. Electroanal. Chem.* **2017**, *799*, 417–423. [[CrossRef](#)]
5. Mortimer, R.J.; Dyer, A.L.; Reynolds, J.R. Electrochromic organic and polymeric materials for display applications. *Displays* **2006**, *27*, 2–18. [[CrossRef](#)]
6. Hsiao, S.H.; Han, J.S. Solution-processable transmissive-to-green switching electrochromic polyamides bearing 2,7-bis(diphenylamino)naphthalene units. *J. Polym. Sci. Part A Polym. Chem.* **2017**, *55*, 1409–1421. [[CrossRef](#)]
7. Montazami, R.; Jain, V.; Heflin, J.R. High contrast asymmetric solid state electrochromic devices based on layer-by-layer deposition of polyaniline and poly(aniline sulfonic acid). *Electrochim. Acta* **2010**, *56*, 990–994. [[CrossRef](#)]
8. Sun, N.; Feng, F.; Wang, D.; Zhou, Z.; Guan, Y.; Dang, G.; Zhou, H.; Chen, C.; Zhao, X. Novel polyamides with fluorene-based triphenylamine: Electrofluorescence and electrochromic properties. *RSC Adv.* **2015**, *5*, 88181–88190. [[CrossRef](#)]
9. Sun, J.; Lv, X.; Wang, P.; Zhang, Y.; Dai, Y.; Wu, Q.; Ouyang, M.; Zhang, C. A donor–acceptor cruciform p-system: High contrast mechanochromic properties and multicolour electrochromic behavior. *J. Mater. Chem. C* **2014**, *2*, 5365–5371. [[CrossRef](#)]
10. Lv, X.; Li, W.; Ouyang, M.; Zhang, Y.; Wright, D.S.; Zhang, C. Polymeric electrochromic materials with donor–acceptor structures. *J. Mater. Chem. C* **2017**, *5*, 12–28. [[CrossRef](#)]
11. Sroog, C.E. Polyimides. *Prog. Polym. Sci.* **1991**, *16*, 561–694. [[CrossRef](#)]
12. Garcia, J.M.; Garcia, F.C.; Serna, F.; Pena, J.L. High-performance aromatic polyamides. *Prog. Polym. Sci.* **2010**, *35*, 623–686. [[CrossRef](#)]
13. Cai, J.; Niu, H.; Zhao, P.; Ji, Y.; Ma, L.; Wang, C.; Bai, X.; Wang, W. Multicolored near-infrared electrochromic polyimides: Synthesis, electrochemical, and electrochromic properties. *Dyes Pigments* **2013**, *99*, 1124–1131. [[CrossRef](#)]
14. Chern, Y.T.; Tsai, J.Y.; Wang, J.J. High T_g and high organosolubility of novel unsymmetric polyimides. *J. Polym. Sci. A Polym. Chem.* **2009**, *47*, 2443–2452. [[CrossRef](#)]
15. Hou, Y.J.; Chen, G.F.; Pei, X.L.; Fang, X.Z. Synthesis and properties of transparent polyimides derived from trans- and cis-1,4-bis(3,4-dicarboxyphenoxy)cyclohexane dianhydrides. *J. Polym. Res.* **2013**, *20*, 159. [[CrossRef](#)]
16. Hsiao, S.H.; Wang, H.M.; Chen, W.J.; Lee, T.M.; Leu, C.M. Synthesis and properties of novel triptycene-based polyimides. *J. Polym. Sci. A Polym. Chem.* **2011**, *49*, 3109–3120. [[CrossRef](#)]
17. Hsiao, S.H.; Hsiao, Y.H.; Kung, Y.R. Synthesis and characterization of new redox-active and electrochromic polyimides with (4-morpholinyl)triphenylamine units. *J. Electroanal. Chem.* **2016**, *764*, 31–37. [[CrossRef](#)]
18. Hsiao, S.H.; Cheng, S.L. New electroactive and electrochromic aromatic polyamides with ether-linked bis(triphenylamine) units. *J. Polym. Sci. A Polym. Chem.* **2015**, *53*, 496–510. [[CrossRef](#)]
19. Hsiao, S.H.; Han, J.S. Redox-active and electrochromic polymers from triarylamine endcapped, 2,7-bis(diphenylamino)naphthalene-cored dicarboxamides. *Eur. Polym. J.* **2017**, *90*, 122–135. [[CrossRef](#)]
20. Liu, H.S.; Pan, B.C.; Huang, D.C.; Kung, Y.R.; Leu, C.M.; Liou, G.S. Highly transparent to truly black electrochromic devices based on an ambipolar system of polyamides and viologen. *NPG Asia Mater.* **2017**, *9*, e388. [[CrossRef](#)]
21. Yen, H.J.; Lin, J.H.; Su, Y.O.; Liou, G.S. Novel triarylamine-based aromatic polyamides bearing secondary amines: Synthesis and redox potential inversion characteristics induced by pyridines. *J. Mater. Chem. C.* **2016**, *4*, 10381–10385. [[CrossRef](#)]

22. Yen, H.J.; Chen, C.J.; Wu, J.H.; Liou, G.S. High performance polymers and their PCBM hybrids for memory device application. *J. Polym. Sci. A Polym. Chem.* **2015**, *6*, 7464–7469. [[CrossRef](#)]
23. Yen, H.J.; Liou, G.S. Solution-processable triarylamine-based electroactive high performance polymers for anodically electrochromic applications. *J. Polym. Sci. A Polym. Chem.* **2012**, *3*, 255–264. [[CrossRef](#)]
24. Ji, Y.; Zhang, C.; Niu, H.; Zhao, X.; Wang, C.; Qin, C.; Wang, W.; Bai, X. Preparation and electrochromic properties of two series of polyurethanes containing separated triphenylamine moiety with different blocks. *Dyes Pigments* **2016**, *125*, 106–115. [[CrossRef](#)]
25. Sun, N.; Zhou, Z.; Meng, S.; Chao, D.; Chu, X.; Zhao, X.; Wang, D.; Zhou, H.; Chen, C. Aggregation-enhanced emission (AEE)-active polyamides with methylsulfonyltriphenylamine units for electrofluorochromic applications. *Dyes Pigments* **2017**, *141*, 356–362. [[CrossRef](#)]
26. Chang, H.W.; Lin, K.H.; Chueh, C.C.; Liou, G.S.; Chen, W.C. New p-type of poly(4-methoxy-triphenylamine)s derived by coupling reactions: Synthesis, electrochromic behaviors, and hole mobility. *J. Polym. Sci. A Polym. Chem.* **2009**, *47*, 4037–4050. [[CrossRef](#)]
27. Jin, G.; Xia, L.; Liu, Z.; Lin, H.; Ling, J.; Wu, H.; Hou, L.; Mo, Y. Highly efficient and stable blue polymer light emitting diodes based on polysilafluorenes with pendent hole transporting groups. *J. Mater. Chem. C* **2016**, *4*, 905–913. [[CrossRef](#)]
28. Yen, H.J.; Lin, K.Y.; Liou, G.S. High T_g , ambipolar, and near-Infrared electrochromic anthraquinone-based aramids with intervalence charge-transfer behavior. *J. Polym. Sci. A Polym. Chem.* **2012**, *50*, 61–69. [[CrossRef](#)]
29. Iwanaga, T.; Ogawa, M.; Yamauchi, T.; Toyota, S. Intramolecular charge-transfer interaction of donor–acceptor–donor arrays based on anthracene bisimide. *J. Org. Chem.* **2016**, *81*, 4076–4080. [[CrossRef](#)] [[PubMed](#)]
30. Wu, J.H.; Liou, G.S. Substituent and charge transfer effects on memory behavior of the ambipolar poly(triphenylamine)s. *ACS Appl. Mater. Interfaces* **2015**, *7*, 15988–15994. [[CrossRef](#)] [[PubMed](#)]
31. Moss, K.C.; Bourdakos, K.N.; Bhalla, V.; Kamtekar, K.T.; Bryce, M.R.; Fox, M.A.; Vaughan, H.L.; Dias, F.B.; Monkman, A.P. Tuning the intramolecular charge transfer emission from deep blue to green in ambipolar systems based on dibenzothiophene *s,s*-dioxide by manipulation of conjugation and strength of the electron donor units. *J. Org. Chem.* **2010**, *75*, 6771–6781. [[CrossRef](#)] [[PubMed](#)]
32. Hsiao, S.H.; Liou, G.S.; Kung, Y.C.; Yen, H.J. High contrast ratio and rapid switching electrochromic polymeric films based on 4-(dimethylamino)triphenylamine-functionalized aromatic Polyamides. *Macromolecules* **2008**, *41*, 2800–2808. [[CrossRef](#)]
33. Ko, Y.G.; Kwon, W.; Yen, H.J.; Chang, C.W.; Kim, D.M.; Kim, K.; Hahm, S.G.; Lee, T.J.; Liou, G.S.; Ree, M. Various digital memory behaviors of functional aromatic polyimides based on electron donor and acceptor substituted triphenylamines. *Macromolecules* **2012**, *45*, 3749–3758. [[CrossRef](#)]
34. Zhou, Y.; Lee, N.A.; Ngo, K.T.; Peng, X.; Feng, Y.; Rochford, J. Rigid triarylamine donor– π –acceptor porphyrin dyes and their application in dye-sensitized solar cells. *RSC Adv.* **2015**, 41193–41202. [[CrossRef](#)]
35. Wang, Y.; Yang, C.; Chen, J.; Qi, H.; Hua, J.; Liu, Y.; Baranoff, E.; Tan, H.; Fan, J.; Zhu, W. Influence of the donor size in panchromatic D– π –A– π –A dyes bearing 5-phenyl-5H-dibenzo-*[b,f]*azepine units for dye-sensitized solar cells. *Dyes Pigments* **2016**, *127*, 204–212. [[CrossRef](#)]
36. Niu, H.; Cai, J.; Zhao, P.; Wang, C.; Bai, X.; Wang, W. Simple approach to regulate the spectra of novel kinds of polyazomethines containing bulky triphenylamine: Electrochemistry, electrochromism and photophysical responsive to environment. *Dyes Pigments* **2013**, *96*, 158–169. [[CrossRef](#)]
37. Niu, H.; Kang, H.; Cai, J.; Wang, C.; Bai, X.; Wang, W. Novel soluble polyazomethines with pendant carbazole and triphenylamine derivatives: Preparation, characterization, and optical, electrochemical and electrochromic properties. *J. Polym. Sci. A Polym. Chem.* **2011**, *2*, 2804–2817. [[CrossRef](#)]
38. Wang, H.M.; Hsiao, S.H. Ambipolar, multi-electrochromic polypyromellitimides and polynaphthalimides containing di(*tert*-butyl)-substituted bis(triarylamine) units. *J. Mater. Chem. C* **2014**, *2*, 1553–1564. [[CrossRef](#)]
39. Ma, X.; Wu, Y.; Wen, H.; Niu, H.; Wang, C.; Qin, C.; Bai, X.; Lei, L.; Wang, W. Immobilized polyazomethines containing triphenylamine groups on ITO: Synthesis and acidochromic, electrochemical, electrochromic and photoelectronic properties. *RSC Adv.* **2016**, *6*, 4564–4575. [[CrossRef](#)]

